Original Paper

Landslides (2024) 21:775–789
DOI 10.1007/s10346-023-02177-6
Received: 24 November 2022
Accepted: 10 November 2023
Published online: 22 December 2023


Emilie Lemaire · Anja Dufresne · Pooya Hamdi · Bretwood Higman · Gabriel J. Wolken · Florian Amann

# Back-analysis of the paraglacial slope failure at Grewingk Glacier and Lake, Alaska

**Abstract** The relationship between rock-slope failure and glacier retreat is complex, and paraglacial failures often lack clearly identified triggers. To better understand the role of glacier retreat in rock-slope failures, we analysed the processes that led to the October 1967 Grewingk landslide in Kachemak Bay State Park on the Kenai Peninsula, Southcentral Alaska. The rock material collapsed onto the glacier toe and into its pro-glacial lake and produced a tsunami wave that swept the outwash plain. On the day of the failure, rainfall and snowmelt were well within normal ranges, and seismic records show no significant shaking. Three years prior to the 1967 failure, the slope withstood the second largest earthquake ever recorded (Great Alaskan earthquake, $M_W$ 9.2). We reassessed the volume of the failure by differencing pre- and post-digital terrain models and found a value of $20–24 \times 10^6$ m$^3$, which is four times smaller than a previous estimate. The back analysis of the Grewingk landslide is based on remote sensing data and field measurements including aerial satellite image analysis, detailed surveying and understanding of the structural geology, a kinematic analysis, and runout modelling. Our research provides an example of a major paraglacial failure that lacks an obvious trigger and points to several geological factors and changing environmental conditions that likely promote such failures. This study further indicates that the Grewingk landslide, pre-conditioned by the geometry of faults and joints, may have reached a critical stability state due to internal processes and the potential combined effects of seismic activity and glacier retreat prior to the collapse.

**Keywords** Landslide · Glacier · Earthquake · Progressive failure · Runout analysis · Alaska

## Introduction

Rock-slope failures are common phenomena in glacial and paraglacial environments. In the last decade, glacier retreat and landslide occurrence has become a prominent research topic, in particular the spatio-temporal relationships between glacier thinning and retreat and rock-slope collapse (e.g. Evans and Clague 1994; Oppikofer et al. 2008; Huggel et al. 2012; Kos et al. 2016; Coe et al. 2018; Higman et al. 2018; Rechberger et al. 2021). Paraglacial slope failures are defined as failures affected by the transitional conditions between glacial and non-glacial conditions (McColl 2012); "paraglacial" specifically refers to "non-glacial processes that are directly conditioned by glaciation" (Church and Ryder 1972; cf. Slaymaker 2009). Recent studies of large deep-seated landslides have documented a correlation between glacier retreat and the acceleration of landslides, highlighting both the stabilizing function of the glacier on the slope flank and a notable delay of up to several years in landslide response after glacier retreat (e.g. Kos et al. 2016; Dai et al. 2020; Storni et al. 2020; Lacroix et al. 2022). The combined impact of debuttressing and climatic factors can also affect the stability of slopes, as demonstrated by Huggel et al. (2012). Furthermore, investigations by Grämiger et al. (2017) have emphasized the importance of ice-loading history in understanding landslide dynamics. The role of ice-thaw in fractures has also been recognized as a contributing factor to landslide stability, as highlighted by Hilger et al. (2021). Hence, the interaction between debuttressing, climatic forcings, ice loading, and thawing of ice within fractures can affect the overall stability of slopes. Additionally, as discussed by Chiarle et al. (2021), the increase in pore water pressure resulting from ice melting in fractures at depth has been identified as an additional factor in slope degradation. Retreating glaciers prepare (e.g. erosion, change in slope hydrology and geometry, fracture development) and can trigger (e.g. debuttressing, fracture daylighting) rock slope instability (e.g. Ballantyne et al. 2014; Holm et al. 2004; Kos et al. 2016; McColl 2012; McColl and Draebing 2019). Here, the term "trigger" refers to the final action that initiates failure of a marginally stable slope. In the slope-stability strength-degradation process, cumulative factors acting as preconditioning elements over time are crucial and may lead to a critical stability state (Stock et al. 2012; Collins and Stock 2016). The term "progressive" refers to time-dependent factors that reduce rock slope stability and may lead to failure (Terzaghi 1950; Stock et al. 2012). While glacier retreat is the most prominent factor in paraglacial slope failure, slopes formerly covered by a glacier and subject to glacial erosion show a range of different failure mechanisms and timing (Ballantyne 2002; Spreafico et al. 2021), and many of these rock-slope failures still lack identified, specific triggers.

To better understand the spatio-temporal (and causative) relationship of glacier retreat and other cumulative processes on slope stability, we studied the 1967 landslide at the retreating Grewingk Glacier in Kachemak Bay State Park, southcentral Alaska. Alaskan glaciers, like most glaciers worldwide, are experiencing rapid and increasing mass loss (Hugonnet et al. 2021), an effect that is enhanced in lake-terminating glaciers compared to those terminating on land (Brun et al. 2019; Tsutaki et al. 2019; Yang et al. 2020; Zhang et al. 2023). In addition, where deep lakes (or fjords) lie below these slopes, rock-slope failures can trigger tsunamis that release destructive energy over a larger area, with larger potential impact on humans, infrastructure or wildlife (e.g. Lituya Bay in 1958: Miller 1960; Grewingk Lake 1967: Wiles and Calkin 1992; Taan Fiord in 2015: Higman et al. 2018). Nearly all Alaskan glaciers show an increased rate of mass loss over the past few decades of accelerated warming (Arendt et al. 2002; Larsen et al. 2015), and there is evidence of

an increase in frequency and size of rock-slope failures in, e.g. Glacier Bay National Park and Preserve, southeast Alaska (Coe et al. 2018). Recent paraglacial rock-slope failures in Alaska include Grewingk Glacier (1967; Wiles and Calkin 1992), Taan Fiord (2015; Higman et al. 2018) and Lamplugh Glacier (2016; Dufresne et al. 2019, and a failure at the same site in 2022; Petley 2022). Wiles and Calkin (1992) have studied the impact of the 1967 Grewingk landslide and its tsunami wave, but did not focus on the slope failure and the factors contributing to the landslide at this place and time. The 1967 slope failure at Grewingk Glacier is an opportunity to investigate the direct influence of glacier retreat on slope destabilization and explore other contributing factors. The rapid and accelerating retreat of the glacier since its Little Ice Age maximum extent in the mid-1800s and a hitherto unknown trigger for its failure makes the area ideal for studying paraglacial slope processes. Through the in-depth analysis of this specific case study, we aim to contribute to a more profound understanding of the direct (or indirect) influence of glacier retreat on slope stability and other slope destabilization processes. To achieve this, we (i) reviewed the estimated volume, (ii) analysed the failure conditions (e.g. geological structures, seismicity, and rainfall), and (iii) investigated the failure sequence by back-analysing the slope failure based on detailed field measurements, a wealth of aerial and satellite images, structural mapping, kinematic analysis, and runout modelling.

## Overview of the study area

### The 1967 Grewingk Landslide

The study site (lat: 59.5929°, long: − 151.1153°) is situated in Kachemak Bay State Park on the Kenai Peninsula, Southcentral Alaska (Fig. 1). The landslide originated from the north-facing slope of Alpine Ridge, directly above the Grewingk proglacial lake. The 1967 landslide scarp is situated above the lake and has a width of 750 m and spans 600 m of elevation. The Grewingk landslide occurred during the early morning of October 14, 1967 (Anchorage Daily times 1967a, b; The Homer News 1967). The rock mass collapsed into the lake and partly onto the glacier toe. The part that collapsed into the lake produced a tsunami wave that stripped trees from the hillside up to an elevation of 60 m above lake-level and surged through the valley, moving boulders and stranding icebergs (Wiles and Calkin 1992). The event did not cause any casualties; however, the area that was inundated is now traversed by several popular hiking trails and includes a developed campsite. Today, the landslide deposit is mostly submerged in the lake, except for one larger hummock forming an island and a second hummock that barely protrudes from the lake; the deposit on the glacier's toe took over 39 years to completely disappear (Fig. 11). An obvious trigger of this collapse was not identified, and, based on the morphology of the 1967 landslide scarp, the precise failure sequence of the slope is unknown and may have included multiple distinct failures.

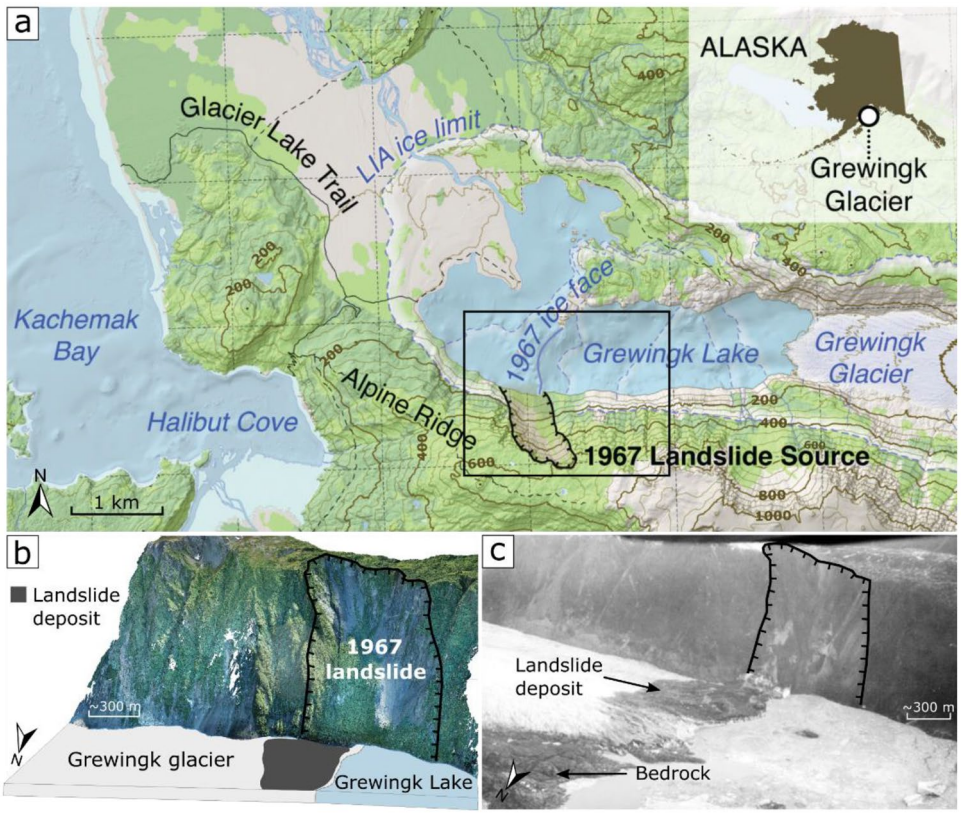


**Fig. 1** **a** Map of the Grewingk area including the 1967 landslide scarp and the location of the site in Alaska. The black rectangle shows the locations of **b** and **c**. **b** 3D reconstruction and representation of the Grewingk Glacier in 1967 with the landslide deposit (point cloud based on data from Corax lln). **c** Photography from 16 October 1967 of the landslide scar (Post 1967)

## Geological and tectonic context

The Kenai Peninsula is crossed by the Border Range fault that separates the fore-arc of Cook Inlet basin in the west and the Chugach terrane accretionary complex in the east (Mankhemthong et al. 2013). The mountains surrounding the 1967 landslide at Grewingk Lake are a classic example of an accretionary wedge, built of highly faulted greywacke crisscrossed by rhyolite dikes (Bradley et al. 1999). The source of the 1967 landslide is located within the McHugh Complex (Fig. 2). It is part of the Chugach accretionary complex, which was mainly built by accretion and underplating processes during subduction along the southern margin of Alaska from the mid-Mesozoic to the Cenozoic (Nokleberg et al. 1989; Plafker et al. 1989; Braden and Behr 2021). The McHugh Complex (KPm) is composed of Triassic to Cretaceous meso-scale deformed tectonic assemblages that include basalt, gabbro, argillite, tuff, greywacke, chert, conglomerate, minor tectonic blocks of limestone and occasionally ultramafic rocks (Bradley et al. 1999; Kusky et al. 2013; Wilson et al. 2015). The predominant lithology within the landslide area is characterized by greywacke. Within the landslide scarp and adjacent slopes, highly fractured rocks and dykes are visible. The surrounding area includes the other packages of the McHugh Complex, KPms and KPmc, that Bradley et al. (1999) locally subdivided and corresponds, respectively, to massive greywacke and conglomerate delimited by faults and to massive basalt covered by chert deposits. Ultramafic plutonic rocks (Tg) and Gabbro (Mg) from the Mesozoic are present.

A series of NE-SW striking thrust faults crosses Alpine Ridge (Fig. 2). In the frame of this study, the fault systems on Alpine Ridge were identified based on field investigations and geomorphological mapping on DTM. Beyond the area of the landslide scarp, a series of faults can be observed with roughly two main trends: NE-SW and W-E. Some of these faults appear to cross the 1967 landslide scarp, and some have a strike sub-parallel to the scarp. The latter are significant due to their control as (lateral) release planes of the 1967 landslide.

On the top of Alpine Ridge, about 200 m from the landslide scarp, a water pond is visible on aerial photos. The pond is crossed by several faults and has been drained between 1985 and 1996, suggesting an increased permeability of the faults and continued adjustments in the slope after the failure.

## Seismic context

The Kenai Peninsula is located along the Aleutian-Alaska subduction zone and is affected by large earthquakes (magnitude > 8) that occur on the Alaska megathrust (Li et al. 2013). In 2021, more than 178 earthquakes with a magnitude of 2.5 or greater took place, and between 2011 and 2021, about 180 earthquakes with a magnitude ≥ 4 occurred (U.S. Geological Survey 2022). Three years prior to the Grewingk landslide, on 27 March 1964, the largest earthquake in North American history and the second largest worldwide ever recorded ($M_W$ 9.2) occurred in Prince William Sound. It triggered thousands of snow avalanches and landslides within the Kenai Mountains, the Chugach Mountains, and Prince William Sound (Grantz et al. 1964) and caused tsunamis with run-up heights of up to 67 m along the Chugach coast (Stover and Coffman 1993). Grewingk

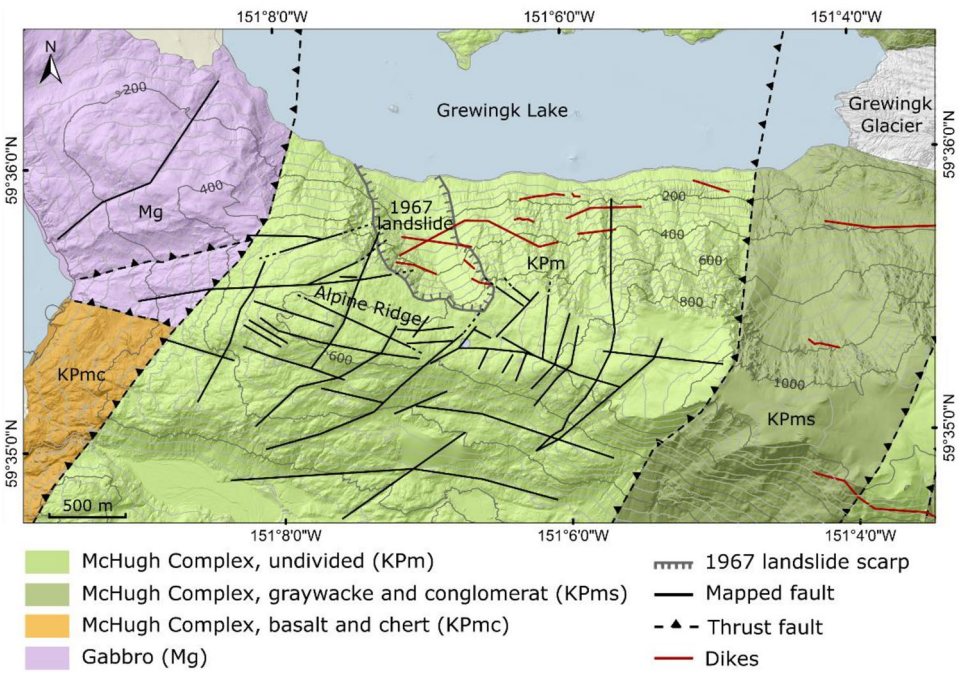


**Fig. 2** Geological map of the Grewingk Lake and Glacier area (modified after Bradley et al. (1999) and Wilson et al. (2015)); mapped faults are based on field observation from this study and geomorphological features, and thrust faults based on Bradley et al. (1999) and Wilson et al. (2015) were approximately located (teeth on upper block)

Glacier and Lake was located directly over the rupture zone of this earthquake (Haeussler et al. 2015) and about 260 km away from the epicentre. The Modified Mercalli Intensity (MMI) at the location of the landslide is estimated to be of 7.1 (U.S. Geological Survey 2020). Homer, located 20 km from Grewingk, was among the areas impacted by slope failures, predominantly slumping or subsidence in unconsolidated sediments (Grantz et al. 1964). Other recorded earthquakes prior to the 1967 landslide at Grewingk Glacier and Lake occurred in November 1959 (M 6.1) at ~ 18 km distance, September 1961 (M 6) at ~ 25 km and August 1967 (M 5.3) at ~ 35 km (U.S. Geological Survey 2022). On the aerial photo from 1964, a fresh landslide deposit at the toe of the slope is evident. The photo was taken 2 months after the Great Alaskan earthquake. It is hence plausible that the earthquake triggered this relatively small collapse ($< 1 \times 10^6$ m$^3$) (Fig. 11a), indicating a significant impact on slope stability.

### Grewingk Glacier history

The Kenai Peninsula is covered by ~3900 km² of glaciers, which correspond to 5% of the total Alaskan glacier area (Yang et al. 2022). Grewingk Glacier trends WNW from the Kenai Mountains to its terminus in its proglacial lake. The retreat of the glacier from its late Pleistocene positions might have started as early as 10,500 years BP (Wiles and Calkin 1992). The area has been the site of at least two large late-Holocene glacial expansions beyond the 1992 margins, the first being from around 1400 years BP and the second during the Little Ice Age advance (Wiles and Calkin 1992). These advances and retreats shaped the lower valley walls with glacial-morphological features such as the lateral moraine, which once stood to roughly 120 m above the current proglacial lake (Wiles and Calkin 1992).

As with most glaciers in Alaska, Grewingk Glacier is currently retreating. Grewingk Glacier started to retreat in 1850 (Wiles and Calkin 1992). A detailed description and a sketch made by W.H Dall and Gilbert (Gilbert 1904) show that by 1900, the glacier had uncovered the lake basin and started being a lake-terminating glacier. Calving accelerated the retreat of the glacier and the lake expanded rapidly. Today, the lake includes many areas of more than 100 m depth. Like many of the glaciers on the Kenai Peninsula (Hall et al. 2005; VanLooy et al. 2006), Grewingk Glacier is undergoing rapid retreat and is retreating faster than the surrounding land-terminating glaciers (e.g. Portlock Glacier, Dixion Glacier, and Wosnesenski Glacier). Between 1899 and 1952, Grewingk Glacier retreated by 0.7 km (Fig. 3). By 1964, it had reached the middle of the later landslide failure area and by 1967 the glacier retreated another ~ 100 m (Fig. 3). The retreat of the Grewingk Glacier has led to an increase in the size and depth of the lake, exposing more of the valley walls.

### Weather and climate condition

The Pacific Ocean moderates the climate in Grewingk area, which is characterised as cold-temperate with cool summers and winters that are freezing and snowy. On average, monthly temperatures range from − 6 °C in January to 16 °C in July (Cedar Lake Ventures Inc 2022). As with other high-latitude locations, Alaska, including the Kenai Peninsula, is warming

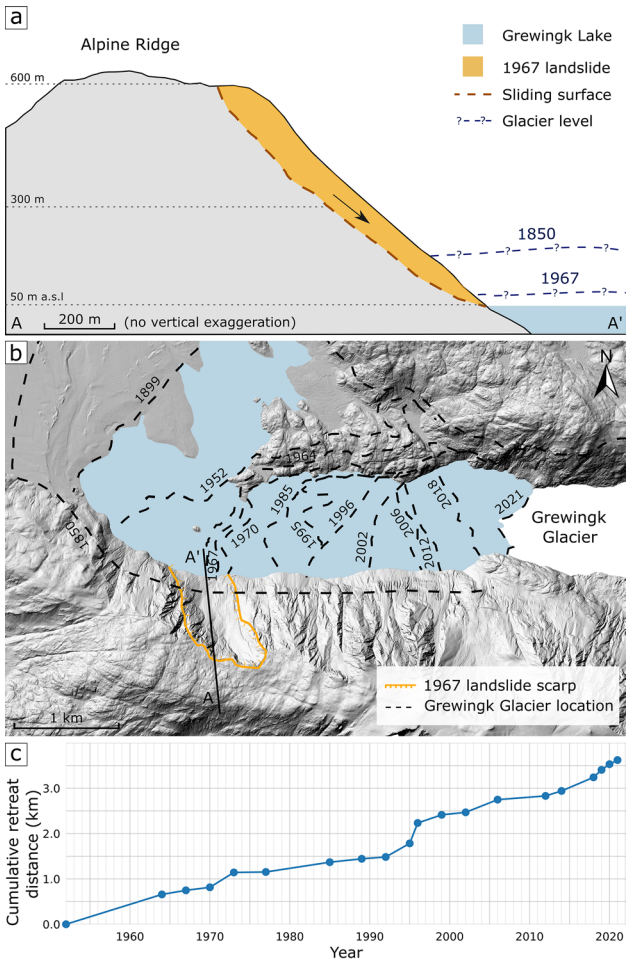


**Fig. 3** **a** Sketch of a profile through the 1967 scarp showing the relationship between glacier thinning and daylighting of the sliding plane/the toe of the landslide mass. The profile is derived from the 1954 DEM from Berthier et al. (2010) and 2019 Lidar (DGGS) **b** Grewingk Glacier retreat evolution through time. **c** Cumulative retreat distance of Grewingk Glacier

nearly four-times the rate as the rest of the globe (Rantanen et al. 2022). From 1951 to 2001, average annual temperatures in Alaska increased by 1.7 °C, with an overall warming rate of 0.16 to 0.37 °C per decade (converted from Alaska Climate Research Center 2020). Permafrost distribution models in Alaska (e.g. Ferrians 1965; Brown et al. 1997; Jorgenson et al. 2008; Pastick et al. 2015) indicate the absence of permafrost in the study area. This absence is likely attributed to the generally moderate mean annual air temperature of the region, which hovers above 1 °C (Ferrians 1965).

For our study area, total precipitation data is available from the European Centre for Medium-Range Weather Forecasts's (ECMWF) Reanalysis v5 (ERA5) on a monthly and daily basis (Figs. 4 and 5). The ERA5 data estimates hourly a wide range of atmospheric, land and oceanic climate variables with a spatial resolution of 0.25° latitude by 0.25° longitude. We analysed their data from year 1950 to year 2021. The monthly results (Fig. 4) show that the 2 months preceding the 1967 Grewingk landslide were the rainiest months of all years: August 1967 with 315 mm and September 1967 with a

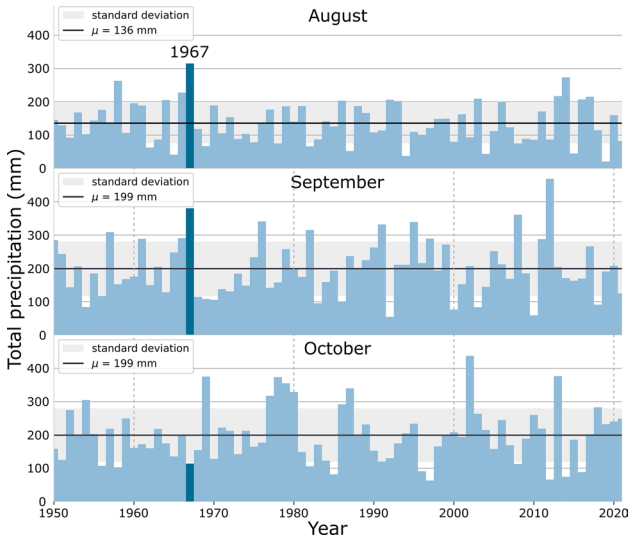


**Fig. 4** Total precipitation (mm) graphs of August, September and October from 1950 to 2021

total precipitation of about 381 mm. In all the years analysed, only 2012 exceeds these values for September. October 1967, the month of the event, recorded ~ 114 mm. Compared to the average of 199 mm from 1950 to 2021, this is a low value. There was no heavy rainfall on the day of the landslide nor during the entire month of October 1967 (Fig. 5).

## Data collection

To reconstruct the deformation history of the slope and the changes of Grewingk Glacier, we analysed available imagery and topographic data that go back to the 1950s (Table 1). The photographs were stacked and georeferenced with control points based on a georeferenced raster of the area and in combination with a second-order polynomial transformation to shift and warp the dataset to its correct location.

An extensive collection of pictures of the landslide scarp and its surrounding were collected in 2018 using a camera (Canon EFS 24 mm on a Canon EOS Rebel SL2) from low-elevation plane and in 2021 using an unmanned aerial vehicle (UAV), DJI Phantom 4. In addition, we collected aerial photos on Alpine Ridge in September 2021 using a DJI Mavic Pro drone. High-resolution topographic data of the landslide and surrounding slopes were produced by photogrammetric analyses using structure-from-motion (SfM). A dense point cloud was created for each of these surveys using the SfM software Agisoft Metashape. A 16-cm resolution DEM, georeferenced with ground control points, was produced from the drone imagery. The imagery dataset from 2018 and the dataset from September 2021 (data from Corax lln) were georeferenced based on the camera position using GPS. The 2019 photogrammetry survey was conducted by Mark Laker of the US Fish and Wildlife Service, Kenai National Wildlife Refuge. These data will later be used to collect structural measurements in areas not accessible by foot.

Grewingk Lake bathymetry was collected in 2019 primarily using a Lawrence single-beam depth sounder mounted to a small raft paddled in transects within the lake by Ed Berg of the University of Alaska Anchorage. This dataset, combined with isolated point plumb-line measurements and the lake shore, was interpolated using a TIN to produce a bathymetric DEM with a pixel resolution of 5 m and was used for the run-out modelling.

## Results

### Structural and kinematic analyses

Rock mass characterisation and structural mapping were carried out using both field observations and remote sensing methods to identify dominant structures affecting slope stability. In total, 546 structural measurements were collected on Alpine Ridge in the summer of 2021 using conventional structural mapping. Besides that, additional 130 measurements were made in a photogrammetry point cloud generated from drone photos using CloudCompare software (CloudCompare 2021). These remote measurements were used in inaccessible steep areas (such as on the steep slope along the ridge, and within the landslide body and scarp), and they show joint-set orientations that are consistent with trends obtained from field measurements (Fig. 6). Stereographic projection analysis was performed, wherein discontinuities were plotted on equal-area stereonets (lower hemisphere) with pole-to-plane Schmidt density contours to identify orientation patterns and main fracture sets.

Structural mapping in the landslide scarp area shows five discontinuity sets (Fig. 6) following essentially two trends: N-S and E-W. J1 has an average dip direction of 10° and dips to the north at 60–80°. The J2 joint set displays an average dip direction of 295° and dips west between 40 and 70°. J3 has an average dip direction of 100° and a dip angle ranging from 40 to 70° towards the east. J4 and J5 are sub-vertical joint sets exhibiting an average dip direction of, respectively, 27° and 165° with a dip angle from 80 to 90° towards the northeast and south. The two main trends

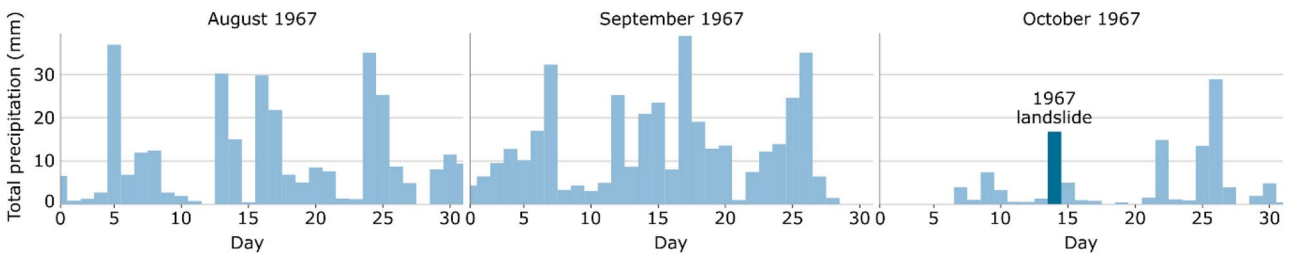


**Fig. 5** Daily total precipitation (mm) graphs in August, September and October 1967

**Table 1** Database imagery for Grewingk Glacier and Lake

| Dataset/source | Year(s) | Data type/method | Resolution(m) |
|---|---|---|---|
| Gilbert sketch | 1899 | Oblique artist drawing | n/a |
| USGS section map | 1951 | Manual photogrammetry | ~100 |
| USGS photos | 1951 | Near-nadir imagery, high-altitude b/w aerial photography | ~20 |
| | 1952 | | ~15 |
| | 1964 | | ~5 |
| Austin Post | 1967 | Photographs | n/a |
| USGS quad map | 1970 | Manual photogrammetry | ~200 |
| AHAP photos | 1985 | Near-nadir imagery, high-altitude false-colour infrared photography | ~5 |
| Landsat | 1972–2022 | Multispectral satellite imagery | 30 |
| USGS ortho quad | 1996 | Aerial ortho-photos | 1 |
| Bathymetry | 2017 | Elevation | Variable |
| Airphoto SfM | 2018 | Photogrammetry on handheld DSLR, low-elevation plane | 0.13 |
| Airphoto SfM | 2019 | Near-nadir photos from low-elevation plane | 0.34 |
| DGGS Lidar | 2019 | Lidar from low-elevation plane | 0.5 |
| DGGS Lidar | 2021 | Lidar | 1 |
| Airphoto SfM | 2021 | Drone images | 0.16 |

of the faults (NE-SW and W-E) have similar orientation to J2, J3 (NE-SW) and J1, J4 (W-E), respectively.

The kinematic method we used to assess the structural data considers that the discontinuities are persistent, dry, and cohesionless, and the individual rock blocks are assumed rigid (Wyllie and Mah 2004). In this analysis, lateral constraints and external forces on the blocks are not taken into account. We completed a kinematic sensitivity analysis for planar sliding, flexural toppling, and wedge failure. For the planar sliding, we assumed lateral limits deviating between 20 to 30° from the slope dip direction (Wyllie and Mah 2004). For the flexural toppling analysis, we set the lateral extents of the critical zone at 20–30° deviation from the slope dip direction (Goodman 1989). For wedge sliding, failure is possible if the intersection of two joint planes dip at an angle lower than the slope angle and greater than the friction angle (Markland 1972). No direct measurement was carried out on shear strength of the discontinuities, but it was concluded that a friction angle in the range of 25–30° would be a reasonable value for kinematic analysis (Wyllie and Norrish 1996). Planar sliding, flexural toppling, and wedge sliding were analysed for an overall slope orientation of 000/55°. For the sensitivity analysis, dip directions between 355 and 15°, and dip angles between 45 and 65° of the slope were assumed. The analysis for the planar failure (Fig. 7a) shows that the joint set J1 would be the main candidate for the failure plane. The analysis for flexural

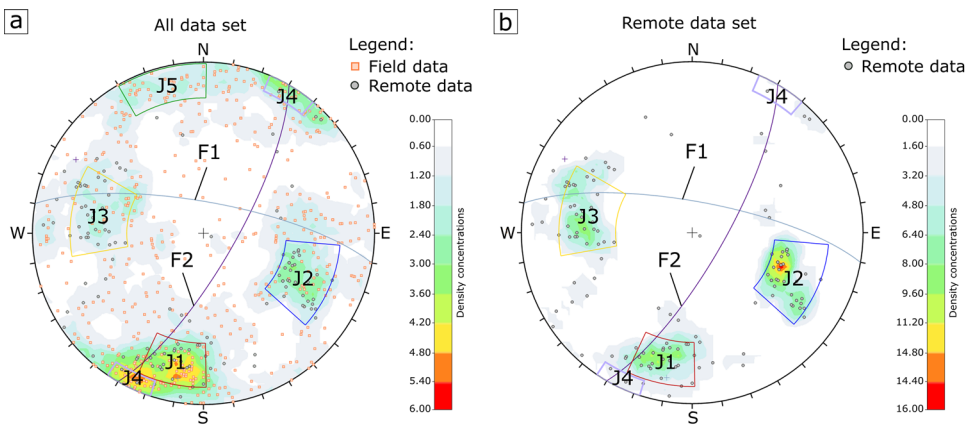


**Fig. 6** Structural analysis based on stereonets with equal area including a all measurements and b measurements taken remotely using UAV. The great circles represent the two main fault families (F1 and F2)

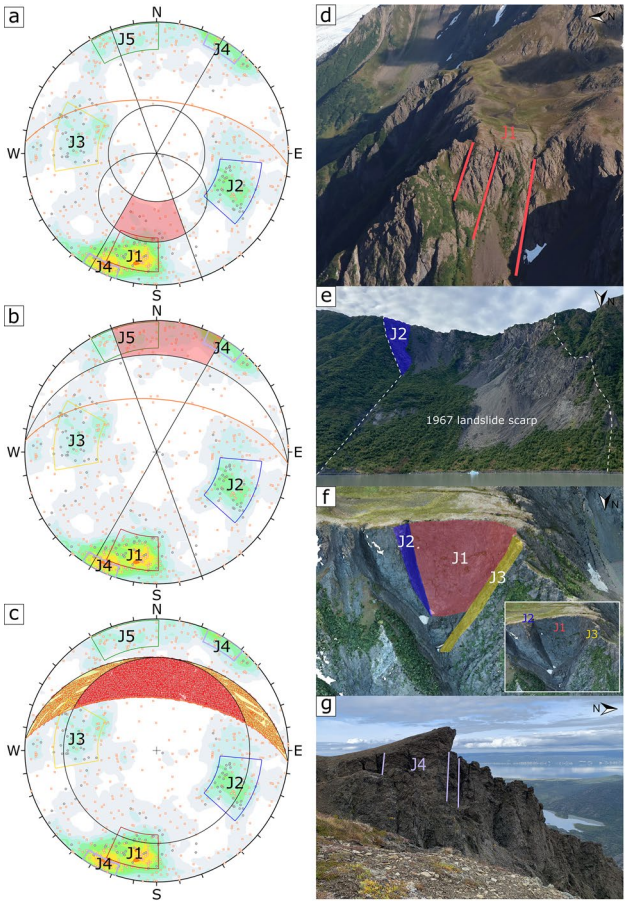


**Fig. 7** Kinematic analysis of **a** planar sliding, **b** flexural toppling and **c** wedge failure. **d** Picture of Alpine Ridge at about 1 km east from the 1967 landslide. **e** Picture facing the 1967 landslide scarp. **f** View on the point cloud (from Corax lln) on Alpine Ridge at about 1 km east from the 1967 landslide scarp. **g** Picture on Alpine Ridge at about 1.5 km east from the scarp

toppling (Fig. 7b) shows that J4 and J5 are critical. The wedge failure analysis (Fig. 7c) shows the highest percentage of critical joints occurring along the intersections of discontinuities; here, J1 with J2 and J1 with J3 are critical.

### Single versus multiple failure mass(es)

We reassessed the volume of the failure of the 1967 landslide based on the difference between the 1954 Digital Elevation Model (DEM) interpolated from the 1954 USGS topographic map (Berthier et al. 2010) and the Lidar collected in 2019 (DGGS, cf. Table 1) (Fig. 12). The calculations were carried out using the software CloudCompare. We, first, performed a fine registration of the two DEMs to ensure accurate alignment. Then, we cropped the DEMs to focus exclusively on the landslide area. Finally, we determined the volume difference between the two DEMs. The total volume released during this event was recalculated to be approximately $22 \times 10^6$ m$^3$ (with an uncertainty of $\pm 2 \times 10^6$ m$^3$), which contrasts with the initial estimation of $84 \times 10^6$ m$^3$ provided by Wiles and Calkin (1992). The uncertainty in estimation arises from the diverse methods used to calculate the complex 3D volume.

Prior to the 1967 slope failure, the crest of Alpine Ridge showed signs of a deep-seated instability, including a well-developed main scarp and a series of scarps and cracks (Figs. 8 and 13). An aerial photo from August 1952 shows a scarp near the base of the slope (Fig. 8a, d). In the mid-slope, a crack had developed and was followed by a slope collapse on the image of March 1964 (Fig. 8b, e). Its deposit covered the base of the slope and the toe of the glacier. On the crest of the slope, the tension crack that released a part of the mass that collapsed in 1967 is noticeable on images from 1952 onwards (Fig. 8). Other tension cracks visible on the 1952 image are still visible on recent aerial photos.

After the analysis of the morphology of the 1967 landslide scarp, we considered two different scenarios: the first (A) assumes that the collapse occurred in a single mass of about $22.5 \times 10^6$ m$^3$ and the second (B) that the mass failed in two phases (Fig. 9). For scenario B, the first phase is the collapse of the western part of the slope with a volume of ~ $8.7 \times 10^6$ m$^3$. Because of kinematic constraints, this first phase is considered as the key element to enable the release of the rock mass in the east part corresponding to the second phase of the failure with a volume of around $11.6 \times 10^6$ m$^3$. Both assumed scenarios are kinematically possible.

### Runout modelling

Runout modelling using DAN3D (cf. McDougall and Hungr 2004) was carried out to assess the two scenarios based on the runout distance and deposit spatial distribution. The pre-failure topography of scenario (A) is based on the 1954 Digital Elevation Model from Berthier et al. (2010) with a pixel resolution of 40 m, whereas the post-failure topography is based on the 2019 Lidar (DGGS). The 2019 Lidar was downsampled to match the resolution of the 1954 DEM of 40 m. The Lidar was modified to represent the glacier at its location in 1967 and the reconstructed pre-failure lake bathymetry based on 2019 bathymetry. For scenario (B), we created two runout models. In the first one, the same initial conditions are used as in scenario (A), except that the failure mass is a smaller wedge failure on the western part of the scarp. For the second mass in scenario (B), the pre-failure topography corresponds to the 1954 DEM minus the first mass that collapsed, and the post-failure topography is the resulting topography of the runout model of the first mass.

A frictional rheology was assumed which required the unit weight, a friction angle, a pore-pressure coefficient and an internal friction angle as input (Table 2). The selection of the initial material properties for the Grewingk landslide was based on literature review from published data on similar sites (Sosio et al. 2008; Si et al. 2017; Penna et al. 2017) and fine-tuned to reproduce the runout distance and lateral spreading of the rock mass (following methods in Claude et al. 2014; Sosio et al. 2012). To consider potential pore-pressure effects, the coefficient Ru was assumed 0 for dry conditions and 0.2 for wet conditions. The latter assumption is based on our sensitivity analysis. The pore pressure (Ru) is an essential parameter affecting runout distances (e.g. Penna et al. 2017). As the saturation of the materials increases, the propagation distance also increases.

In both scenarios A and B, the rock mass collapsed into the lake and partly ran out over the toe of the glacier at about the

same distance up to 500 m. For scenario (A), we estimated the deposit volume over the glacier toe at about $3 \times 10^6$ m$^3$. The results for scenario (B) show that both masses from the eastern and western part are propagating into the lake and over the glacier. However, the mass of the eastern part is the main contributor to the deposit on the glacier's toe with a volume of about $2 \times 10^6$ m$^3$. The rock material of the western part has spread on the glacier toe to a distance up to 16 m and with a volume of around $0.5 \times 10^6$ m$^3$. The runout modelling results for the two different scenarios and the two different conditions, dry and wet, show similarities (Fig. 10). The results of the DAN3D successfully reproduce the deposit runout distance and lateral spreading; hence, both scenario are equally possible based on this.

## Discussion

To investigate the relationship between glacier retreat and the 1967 landslide, we analysed the main influencing factors and potential triggers (including structural geology, glacier debuttressing, rainfall, and seismicity) and their spatio-temporal relationship to thinning, retreat and dynamics (grounded versus floating) of Grewingk Glacier.

The kinematic analysis together with structural features shows that the collapse was structurally controlled. The failure mass was laterally released along the orientation of joint sets J2 and J3. However, joints do not usually have the persistence to form lateral release planes on such a scale. Faults are often persistent for much more than 100 m. Lateral release planes are, therefore, most likely related to faults with the same orientation of J2 and J3 that are present within the study area (cf. Fig. 7). The exact failure mechanism remains unclear because the joint orientations allow a variety of failure modes. It is likely that the collapse of such a highly fractured ridge (cf. Fig. 2) occurred not in one simple failure mode, but rather a more complex failure. By integrating kinematic considerations with geomorphological features, such as tension cracks, scarps and fault traces and the scale of the landslide, the lateral extent of the 1967 landslide is most likely determined by persistent faults in a J2 and J3 orientation. The failure mode, controlled by the various joint sets with lower persistence, may vary locally depending on variations of the slope and structure geometries as well as mechanical joint-set characteristics (e.g. persistence). Several scarps and tension cracks were visible before the event and some are still present pointing to a longer-term and ongoing slope adjustment.

Grewingk Glacier has undergone changes and receded rapidly over the years, influencing the surrounding slopes. Glaciers erode slope flanks, remove the support on the rock walls, redistribute stress, deposit debris in form of moraines and uncover persistent geological structures, all of which can facilitate failure (e.g. Braathen et al. 2004; Geertsema et al. 2014; Spreafico et al. 2021). Several studies have demonstrated that the response of rock slopes to deglaciation occurs over a wide range of time-scales up to thousands of years (e.g. Evans and Clague 1994; Lacroix et al. 2022). When a slope is affected by debuttressing, the loss of lateral confinement or support can result in stress redistribution within the slope mass, exposing the rock mass to variation in surface temperature and pore pressure (Storni et al. 2020). Relaxation of internal stresses due to glacier retreat (e.g. Evans and Clague 1994) may facilitate crack initiation or growth (e.g. Fischer et al. 2010; Ballantyne et al. 2014), including slope-parallel unloading

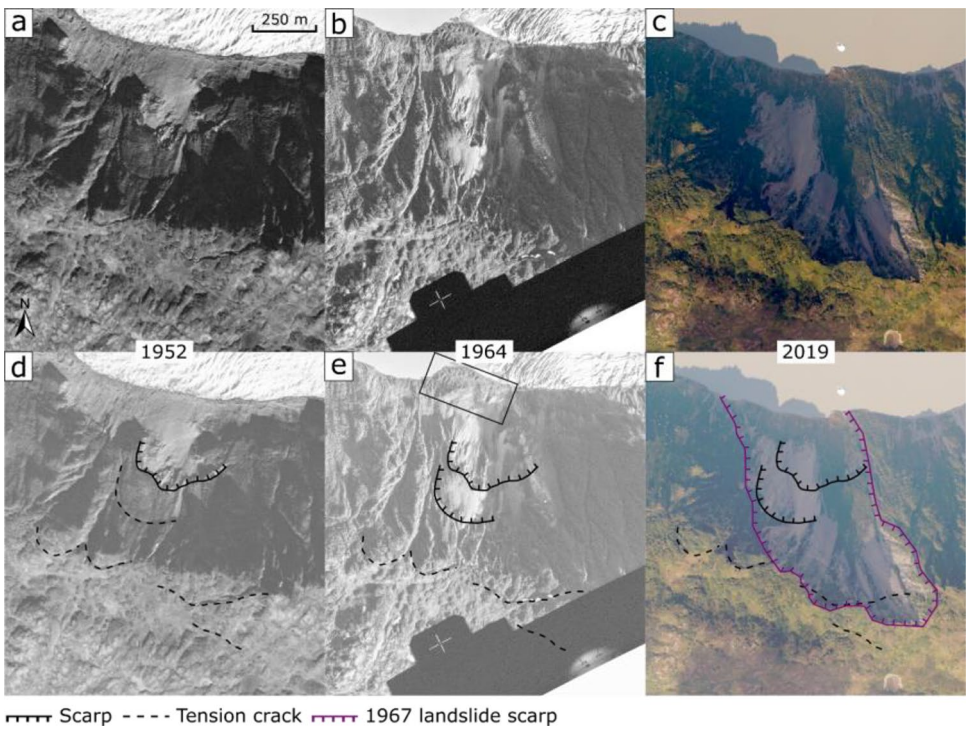


**Fig. 8** Slope, of the 1967 event, evolution through time. **a**, **d** Pre-failure Aerial Photo Single Frame from 15.08.1952 (image courtesy of the U.S. Geological Survey). **b**, **e** Pre-failure Aerial Photo Single Frame from 29.08.1964 (image courtesy of the U.S. Geological Survey); the black rectangle indicates a deposit from a shallower landslide. **c, f** Post-failure orthmosaic 2019 (from M. Laker). For a more detailed view of the features, see Fig. 13

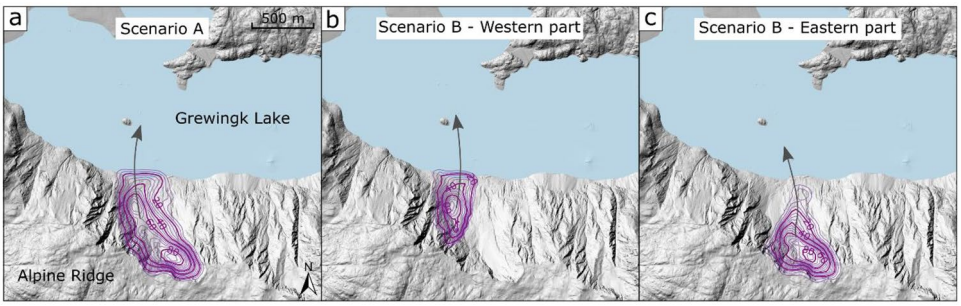


**Fig. 9** Single versus two masses failure with **a** scenario A, **b** scenario B with the first mas and **c** scenario B with the second mass

fractures (Nichols 1980; Leith et al. 2014). Grämiger et al. (2017) investigated the effect of long-term ice-loading over successive glacial cycles, extending over thousands of years, on the development of rock damage within the rock mass. They found that this prolonged ice-loading plays a crucial role that can lead to a long-term degradation of the stability. Hence, the relationship between glacier retreat and rock-slope collapse is not so straightforward. Glacier retreat can act as either a preparatory factor or a trigger (Grämiger et al. 2017; Storni et al. 2020). Grewingk Glacier started to retreat in 1850; by 1964, it had reached the middle of the later landslide failure area. In the same year of the landslide event, in 1967, the glacier retreated another ~ 100 m from its 1964 position (Fig. 5). Although this significant retreat of the glacier prior to the catastrophic failure in 1967 may suggest a direct relationship between glacier thinning and slope failure, the slope stability history is more complex, particularly in areas that are affected by a variety of potential landslide triggers and preparatory factors, such as high seismic activity.

In mountainous areas, earthquakes can trigger widespread landslides (Keefer 1984; Gorum et al. 2011; Marc et al. 2015) and decrease rock slope stability. Keefer (1984) and Rodríguez et al. (1999) showed that the critical magnitude to trigger landslides is $M_L = 4$, and the number of collapses increases with the earthquake magnitude; the number and distribution of landslides vary as a function of the distance from the seismic source. A single earthquake can trigger more than several thousands of landslides

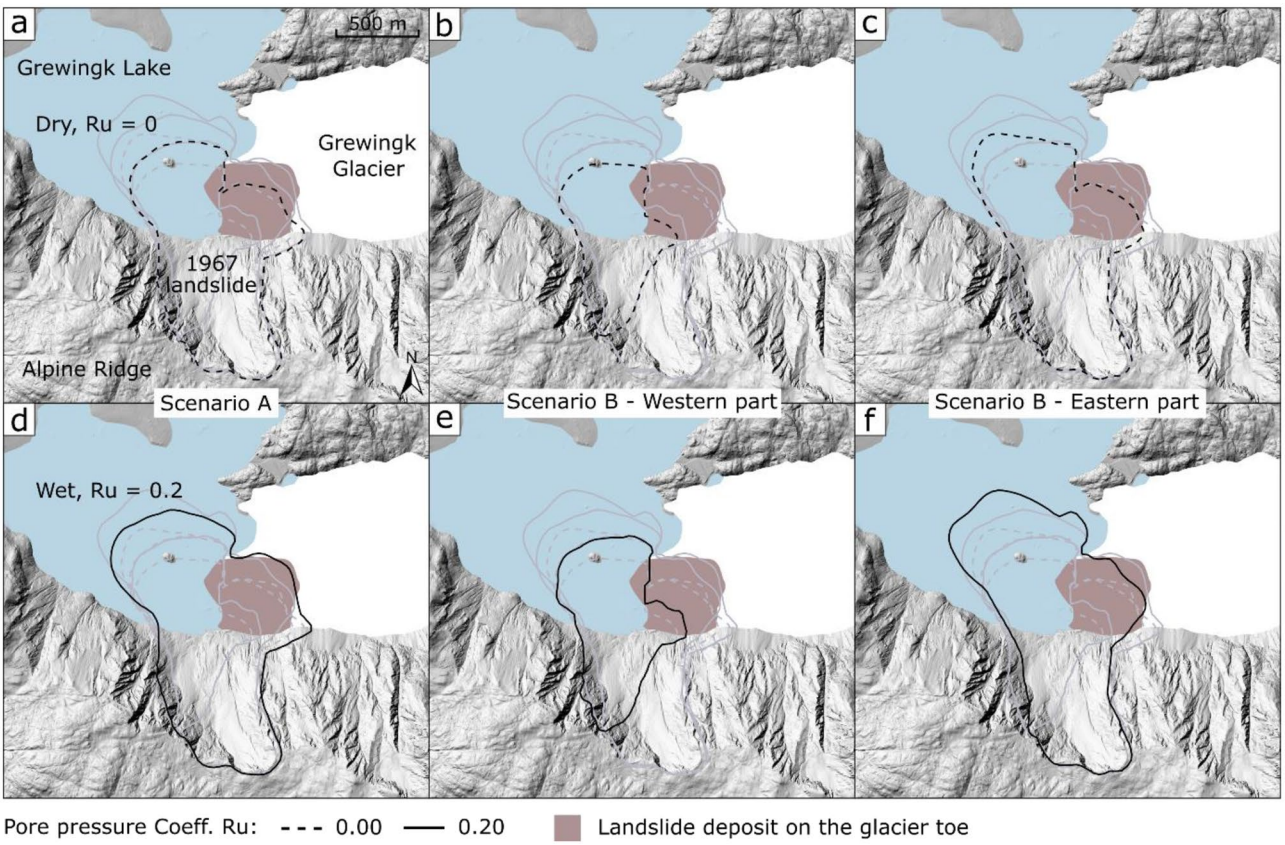


**Fig. 10** Results of the DAN3D runout modelling for **a** scenario A with a pore pressure of 0, **b** scenario B (first mass) with a pore pressure of 0, **c** scenario B (second mass) with a pore pressure of 0, **d** scenario A with a pore pressure of 0.2, **e** scenario B (first mass) with a pore pressure of 0.2 and **f** scenario B (second mass) with a pore pressure of 0.2

**Table 2** Input parameters to DAN3D runout analysis

| Material type | Unit weight (kN/m³) | Friction angle φ | Pore-pressure coeff. Ru | Internal friction angle $\varphi_c$ | Condition |
|---|---|---|---|---|---|
| Frictional | 25 | 25° | 0 | 35° | Dry |
| Frictional | 25 | 25° | 0.2 | 35° | Wet |

over a distance up to several hundred kilometres away from the epicentre (e.g. Havenith et al. 2016; Fan et al. 2018). Moreover, the cumulative effect of seismicity over time can affect and weaken rock slopes (Moore et al. 2012; Stead and Wolter 2015; Gischig et al. 2015, 2016). Earthquake-triggered landslides are not limited to the immediate aftermath of an earthquake, but can also occur after a considerable lapse of time (Keefer 1984; Bontemps et al. 2020). The mechanisms and occurrence of post-seismic landslides (e.g. Yang et al. 2017; Brain et al. 2021; Illien et al. 2022) can be attributed to several factors, including ground shaking, changes in pore water pressure, groundwater level fluctuation, and the weakening of slopes due to the redistribution of stresses during the earthquake event (Brain et al. 2021; Illien et al. 2022). Three years prior to the Grewingk landslide, the 1964 Great Alaskan earthquake struck Alaska and triggered numerous landslides across the affected region; among these, 75 rock avalanches were documented (Post 1967). In the years following the 1964 earthquake, additional landslides occurred (e.g. Fairweather and Allen landslides). These landslides share similarities in characteristics to the rock avalanches that occurred at the time of the 1964 Great Alaskan earthquake (Post 1967). For example, the Fairweather landslide, which occurred in the Fairweather Range near Glacier Bay National Park and Preserve in 1965, is a major event in the region's landslide history. The slope of the Grewingk landslide sits directly over the rupture zone of the 1964 Great Alaskan earthquake (Haeussler et al. 2015), and a MMI of 7.1 was estimated for the site (U.S. Geological Survey 2020). Hence, situated in a seismically highly active area, with four earthquakes > M5 in the decade preceding the 1967 slope failure, an adverse impact of seismicity on slope stability cannot be ruled out.

Besides earthquakes, rainfall is one of the most common triggers of landslides (Iverson 2000; Chen and Lee 2003; Dahal and Hasegawa 2008), and Rodríguez et al. (1999) argue "that rainfall-induced and earthquake-induced landslide hazards should be assessed simultaneously". Rainfall-induced landslides occur after intense or long rainfalls, depending on the type of landslide and antecedent slope saturation (Iverson 2000; Chen and Lee 2003; Balzano et al. 2019). The response of landslides to rainfall varies, some slopes collapse suddenly and travel a long distance at high velocity, while others respond and move slowly (Iverson 2000). The combined effect of earthquakes and rainfall can impact the kinematic behaviour of slopes over time (Bontemps et al. 2020). The occurrence of small earthquakes in addition to precipitation prolongs the critical regime of the landslide compared to seismic quiescence (Bontemps et al. 2020). At Grewingk, ERA5 reanalysis shows unusually high precipitation for the 2 months before failure. It is unclear if this precipitation may have led to unusually high pore-water pressures in the rock mass. Spring level changes due to precipitation or snow melt of up to 100–200 m in altitude have been documented for many rock slope instabilities (i.e. Amann 2006; Gischig et al. 2011; Moser et al. 2017) and related to fluid pressure changes and accelerated (i.e. up to a factor of two) deformations (Moser et al. 2017). Field observations and careful analysis of aerial photos do not show significant altitude changes of springs at the north exposed slopes above Grewingk Lake suggesting no major water pressure changes in the observable period. This might be associated with an enhanced permeability due to slope deformations and a direct drainage of infiltrating precipitation. Similar observations have been reported by Amann (2006) who found at the Sedrun landslide in Switzerland that the water table in the active rock slope instability is 300–400 m lower than in the adjacent stable ground, associated with an enhanced permeability due to deformations. This interpretation is also corroborated by the observation of a water pond along the ridge right above the 1967 landslide scarp that has been likely drained through slope deformation that opened fractures or faults and thus an enhanced permeability.

Independent of the final trigger, runout modelling showed that a single failure mass or two consecutive failures are both possible scenarios. The latter is more likely from the degree of freedom of the western part of the rock slope compared to the eastern part. To further elucidate the sequences of the events, impulse water wave modelling as well as more detailed bathymetric mapping are planned. The comparison of the run-up distance of the wave from a single large mass versus two smaller masses collapsing into the proglacial lake will help to clarify the failure scenario.

## Conclusion

The 1967 landslide at Grewingk Glacier and Lake demonstrates that there is more to the story of rock-slope failures in paraglacial environments than glacier retreat alone. Results from kinematic analysis and runout modelling show that both a single failure mass and two consecutive failures are possible scenarios. On the day of the Grewingk event, no specific trigger such as intense rainfall, seismic activity, or snow melting is evident. Our study shows that the landslide was conditioned by structural geology with persistent faults laterally constraining the collapse and by various joint sets with lower persistence controlling the internal failure with different potential failure modes. A series of earthquakes caused smaller-scale landslides on the (already unstable) part of the slope that catastrophically failed in 1967. Therefore, the landslide may have reached a critical stability state due to progressive failure prior to 1967, making an analysis of the longer-term spatio-temporal patterns of paraglacial rock slope behaviour/deformation essential. In particular, since no specific trigger can be unequivocally identified, our study stresses the importance to view paraglacial slope failures holistically and expand research beyond the glacier-retreat slope-failure connection. It is a contribution to the regional-scale analysis of paraglacial slope stability where several preparatory factors contributed to a progressive failure in which internal processes, affected over time by preconditioning characteristics and external processes, led to a decrease in the stability of the slope and resulted in the 1967 failure.

## Funding

Open Access funding enabled and organized by Projekt DEAL. Funded by the*Deutsche Forschungsgemeinschaft(DFG, German Research Fundation) – 447808231.*

## Data availability

Data are available from the authors upon request.

## Declarations

**Competing interests** The authors declare no competing interests.

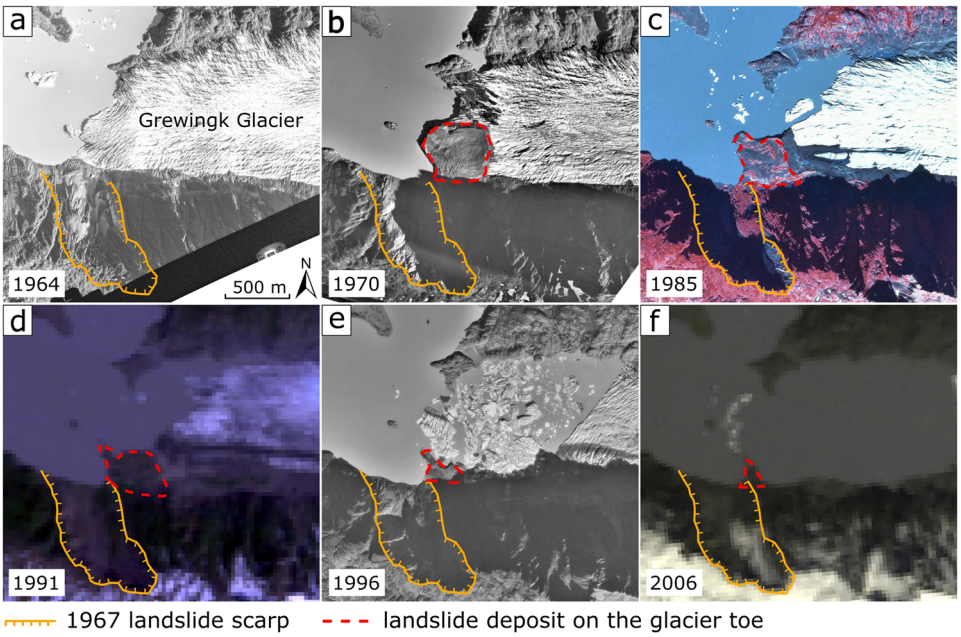


**Fig. 11** Evolution through time of the landslide deposit on the Grewingk Glacier. **a** Pre-failure Aerial Photo Single Frame from 29.08.1964 (image courtesy of the U.S. Geological Survey). **b** Aerial Photo Single Frame from 02.09.1970 (image courtesy of the U.S. Geological Survey). **c** Alaska High-Altitude Photography from 27.08.1985 (image courtesy of the AHAP program). **d** Landsat 4–5 TM C2 from 22.06.1991 (image courtesy of the U.S. Geological Survey). **e** Digital Orthophoto Quadrangle from 03.09.1996 (image courtesy of the U.S. Geological Survey). **f** Landsat 4–5 TM C2 from 23.05.2006 (image courtesy of the U.S. Geological Survey)

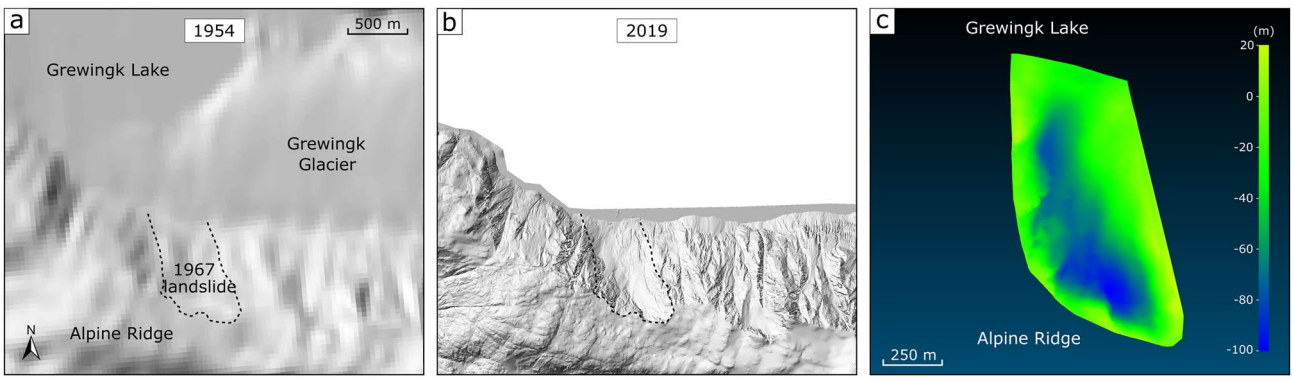


**Fig. 12** Hillshade of the DEMS used for the volume calculation. **a** Pre-failure topography obtained from the 1954 DEM by Berthier et al. (2010). **b** Post-failure topography based on the 2019 Lidar data (DGGS). **c** Result from the 2.5D volume tool from CloudCompare with the color scale indicating the hieght above ground

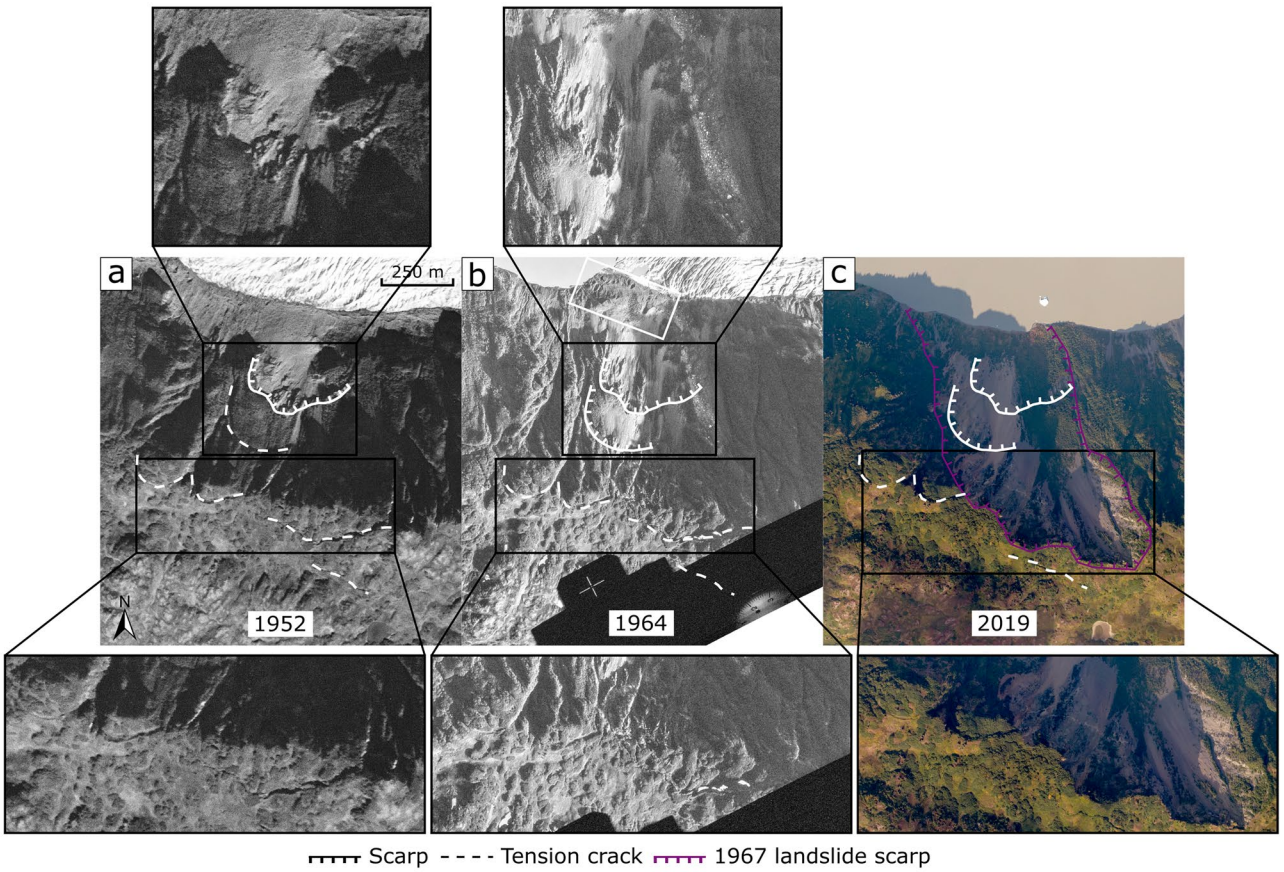


**Fig. 13** Overview of Fig. 8 with additional zooms on features. **a** Pre-failure Aerial Photo Single Frame from 15.08.1952 (image courtesy of the U.S. Geological Survey). **b** Pre-failure Aerial Photo Single Frame from 29.08.1964 (image courtesy of the U.S. Geological Survey); the white rectangle indicates a deposit from a shallower landslide. **c** Post-failure orthmosaic 2019 (from M. Laker)

## Appendix



## References

Alaska Climate Research Center (2020) Climate change in Alaska. https://akclimate.org/climate-change-in-alaska/. Accessed 25 May 2022

Amann F (2006) Großhangbewegung Cuolm Da Vi (Graubünden. Friedrich-Alexander-Universität, Schweiz) Geologisch-geotechnische Befunde und numerische Untersuchungen zur Klärung des Phänomens

Anchorage Daily times (1967a) Glacier behaving strangely, p 2

Anchorage Daily times (1967b) Explosion an ice-slide, p 2

Arendt AA, Echelmeyer KA, Harrison WD et al (2002) Rapid wastage of Alaska glaciers and their contribution to rising sea level. Science 297:382–386. https://doi.org/10.1126/science.1072497

Ballantyne CK (2002) Paraglacial geomorphology. Quatern Sci Rev 21:1935–2017. https://doi.org/10.1016/S0277-3791(02)00005-7

Ballantyne CK, Sandeman GF, Stone JO, Wilson P (2014) Rock-slope failure following late pleistocene deglaciation on tectonically stable mountainous terrain. Quatern Sci Rev 86:144–157. https://doi.org/10.1016/j.quascirev.2013.12.021

Balzano B, Tarantino A, Ridley A (2019) Preliminary analysis on the impacts of the rhizosphere on occurrence of rainfall-induced shallow landslides. Landslides 16:1885–1901. https://doi.org/10.1007/s10346-019-01197-5

Berthier E, Schiefer E, Clarke GKC et al (2010) Contribution of Alaskan glaciers to sea-level rise derived from satellite imagery. Nature Geosci 3:92–95. https://doi.org/10.1038/ngeo737

Bontemps N, Lacroix P, Larose E et al (2020) Rain and small earthquakes maintain a slow-moving landslide in a persistent critical state. Nat Commun 11:780. https://doi.org/10.1038/s41467-020-14445-3
Braathen A, Blikra L, Berg S, Karlsen F (2004) Rock slope failures of Norway: type, geometry, deformation mechanisms and stability. Norw J Geol 84:67–88
Braden Z, Behr WM (2021) Weakening mechanisms in a basalt-hosted subduction megathrust fault segment. Southern Alaska JGR Solid Earth 126:9. https://doi.org/10.1029/2021JB022039
Bradley DC, Kusky TMK, Haeussler PJ et al (1999) Geology of the Seldovia quadrangle. U.S. Geological Survey Open-File Report 99–18, scale: 1:250,000
Brain MJ, Moya S, Kincey ME et al (2021) Controls on post-seismic landslide behavior in brittle rocks. J Geophys Res Earth Surf 126:9. https://doi.org/10.1029/2021JF006242
Brown J, Ferrians OJ Jr, Heginbottom JA, Melnikov ES (1997) Circum-Arctic map of permafrost and ground-ice conditions. U.S. Geological Survey, Map CP-45, scale 1:10,000,000
Brun F, Wagnon P, Berthier E et al (2019) Heterogeneous influence of glacier morphology on the mass balance variability in High Mountain Asia. J Geophys Res Earth Surf 124:1331–1345. https://doi.org/10.1029/2018JF004838
Cedar Lake Ventures Inc (2022) Climate and average weather year round in Homer, Alaska, United States. https://weatherspark.com/y/212/Average-Weather-in-Homer-Alaska-United-States-Year-Round. Accessed 14 Sep 2022
Chen H, Lee CF (2003) A dynamic model for rainfall-induced landslides on natural slopes. Geomorphology 51:269–288. https://doi.org/10.1016/S0169-555X(02)00224-6
Chiarle M, Geertsema M, Mortara G, Clague JJ (2021) Relations between climate change and mass movement: perspectives from the Canadian Cordillera and the European Alps. Global Planet Change 202:103499. https://doi.org/10.1016/j.gloplacha.2021.103499
Church M, Ryder JM (1972) Paraglacial sedimentation: a consideration of fluvial processes conditioned by glaciation. Geol Soc America Bull 83:3059. https://doi.org/10.1130/0016-7606(1972)83[3059:PSACOF]2.0.CO;2
Claude A, Ivy-Ochs S, Kober F et al (2014) The Chironico landslide (Valle Leventina, southern Swiss Alps): age and evolution. Swiss J Geosci 107:273–291. https://doi.org/10.1007/s00015-014-0170-z
CloudCompare (2021) version 2.11.3 (Anoia) [GPL software]. Retrieved from http://www.cloudcompare.org/
Coe JA, Bessette-Kirton EK, Geertsema M (2018) Increasing rock-avalanche size and mobility in Glacier Bay National Park and Preserve, Alaska detected from 1984 to 2016 Landsat imagery. Landslides 15:393–407. https://doi.org/10.1007/s10346-017-0879-7
Collins BD, Stock GM (2016) Rockfall triggering by cyclic thermal stressing of exfoliation fractures. Nature Geosci 9:395–400. https://doi.org/10.1038/ngeo2686
Dahal RK, Hasegawa S (2008) Representative rainfall thresholds for landslides in the Nepal Himalaya. Geomorphology 100:429–443. https://doi.org/10.1016/j.geomorph.2008.01.014
Dai C, Higman B, Lynett PJ et al (2020) Detection and assessment of a large and potentially tsunamigenic periglacial landslide in Barry Arm. Alaska Geophysical Research Letters 47:22. https://doi.org/10.1029/2020GL089800
Dufresne A, Wolken GJ, Hibert C et al (2019) The 2016 Lamplugh rock avalanche, Alaska: deposit structures and emplacement dynamics. Landslides 16:2301–2319. https://doi.org/10.1007/s10346-019-01225-4
Evans SG, Clague JJ (1994) Recent climatic change and catastrophic geomorphic processes in mountain environments. Geomorphology 10:107–128. https://doi.org/10.1016/0169-555X(94)90011-6
Fan X, Juang CH, Wasowski J et al (2018) What we have learned from the 2008 Wenchuan Earthquake and its aftermath: A decade of research and challenges. Eng Geol 241:25–32. https://doi.org/10.1016/j.enggeo.2018.05.004
Ferrians OJ Jr (1965) Permafrost map of Alaska. U.S. geological survey, miscellaneous geologic investigations map 445, scale: 1:2,500,000
Fischer L, Amann F, Moore JR, Huggel C (2010) Assessment of periglacial slope stability for the 1988 Tschierva rock avalanche (Piz Morteratsch, Switzerland). Eng Geol 116:32–43. https://doi.org/10.1016/j.enggeo.2010.07.005
Geertsema M, Clague J, Hasler A (2014) Influence of climate change on geohazards in Alaskan parks. Alaska Park Science 12:81–85
Gilbert GK (1904) Alaska: volume III: glacier and glaciation. Doubleday, Page and Company
Gischig V, Amann F, Moore JR et al (2011) Composite rock slope kinematics at the current Randa instability, Switzerland, based on remote sensing and numerical modeling. Eng Geol 118:37–53. https://doi.org/10.1016/j.enggeo.2010.11.006
Gischig VS, Eberhardt E, Moore JR, Hungr O (2015) On the seismic response of deep-seated rock slope instabilities — insights from numerical modeling. Eng Geol 193:1–18. https://doi.org/10.1016/j.enggeo.2015.04.003
Gischig V, Preisig G, Eberhardt E (2016) Numerical investigation of seismically induced rock mass fatigue as a mechanism contributing to the progressive failure of deep-seated landslides. Rock Mech Rock Eng 49:2457–2478. https://doi.org/10.1007/s00603-015-0821-z
Goodman R (1989) Introduction to rock mechanics, 2nd edn. John Wiley & Sons Ltd., New York
Gorum T, Fan X, van Westen CJ et al (2011) Distribution pattern of earthquake-induced landslides triggered by the 12 May 2008 Wenchuan earthquake. Geomorphology 133:152–167. https://doi.org/10.1016/j.geomorph.2010.12.030
Grämiger LM, Moore JR, Gischig VS et al (2017) Beyond debuttressing: mechanics of paraglacial rock slope damage during repeat glacial cycles: paraglacial rock slope mechanics. J Geophys Res Earth Surf 122:1004–1036. https://doi.org/10.1002/2016JF003967
Grantz A, Plafker G, Kachadoorian R (1964) Alaska's Good Friday earthquake, March 27, 1964, a preliminary geologic evaluation. Geol Surv Circul 491. https://doi.org/10.3133/cir491
Haeussler PJ, Armstrong PA, Liberty LM et al (2015) Focused exhumation along megathrust splay faults in Prince William Sound, Alaska. Quatern Sci Rev 113:8–22. https://doi.org/10.1016/j.quascirev.2014.10.013
Hall DK, Giffen BA, Chien JYL (2005) Changes in the Harding Icefield and the Grewingk-Yalik Glacier Complex. 62nd Eastern snow conference, Waterloo, Canada
Havenith H-B, Torgoev A, Braun A et al (2016) A new classification of earthquake-induced landslide event sizes based on seismotectonic, topographic, climatic and geologic factors. Geoenviron Disasters 3:6. https://doi.org/10.1186/s40677-016-0041-1
Higman B, Shugar DH, Stark CP et al (2018) The 2015 landslide and tsunami in Taan Fiord. Alaska Sci Rep 8:12993. https://doi.org/10.1038/s41598-018-30475-w
Hilger P, Hermanns RL, Czekirda J et al (2021) Permafrost as a first order control on long-term rock-slope deformation in (sub-)Arctic Norway. Quatern Sci Rev 251:106718. https://doi.org/10.1016/j.quascirev.2020.106718
Holm K, Bovis M, Jakob M (2004) The landslide response of alpine basins to post-Little Ice Age glacial thinning and retreat in southwestern British Columbia. Geomorphology 57:201–216. https://doi.org/10.1016/S0169-555X(03)00103-X
Huggel C, Clague JJ, Korup O (2012) Is climate change responsible for changing landslide activity in high mountains?: climate change and landslides in high mountains. Earth Surf Process Landforms 37:77–91. https://doi.org/10.1002/esp.2223
Hugonnet R, McNabb R, Berthier E et al (2021) Accelerated global glacier mass loss in the early twenty-first century. Nature 592:726–731. https://doi.org/10.1038/s41586-021-03436-z

Illien L, Sens-Schönfelder C, Andermann C et al (2022) Seismic velocity recovery in the subsurface: transient damage and groundwater drainage following the 2015 Gorkha Earthquake, Nepal. JGR Solid Earth 127. https://doi.org/10.1029/2021JB023402

Iverson RM (2000) Landslide triggering by rain infiltration. Water Resour Res 36:1897–1910. https://doi.org/10.1029/2000WR900090

Jorgenson M, Yoshikawa K, Kanevskiy M et al (2008) Permafrost characteristics of Alaska. In: In Proceedings of the Ninth International Conference on Permafrost. University of Alaska, Fairbanks, AK, USA, pp 121–122

Keefer DK (1984) Landslides caused by earthquakes. Geol Soc America Bull 95:406. https://doi.org/10.1130/0016-7606(1984)95%3c406:LCBE%3e2.0.CO;2

Kos A, Amann F, Strozzi T et al (2016) Contemporary glacier retreat triggers a rapid landslide response, Great Aletsch Glacier, Switzerland. Geophys Res Lett 43. https://doi.org/10.1002/2016GL071708

Kusky TM, Windley BF, Safonova I et al (2013) Recognition of ocean plate stratigraphy in accretionary orogens through Earth history: a record of 3.8billion years of sea floor spreading, subduction, and accretion. Gondwana Res 24:501–547. https://doi.org/10.1016/j.gr.2013.01.004

Lacroix P, Belart JMC, Berthier E et al (2022) Mechanisms of landslide destabilization induced by glacier-retreat on Tungnakvíslarjökull Area, Iceland. Geophys Res Lett 49. https://doi.org/10.1029/2022GL098302

Larsen CF, Burgess E, Arendt AA et al (2015) Surface melt dominates Alaska glacier mass balance. Geophys Res Lett 42:5902–5908. https://doi.org/10.1002/2015GL064349

Leith K, Moore JR, Amann F, Loew S (2014) In situ stress control on microcrack generation and macroscopic extensional fracture in exhuming bedrock: fracture generation in exhuming bedrock. J Geophys Res Solid Earth 119:594–615. https://doi.org/10.1002/2012JB009801

Li J, Abers GA, Kim Y, Christensen D (2013) Alaska megathrust 1: seismicity 43 years after the great 1964 Alaska megathrust earthquake: ALASKA MEGATHRUST 1. J Geophys Res Solid Earth 118:4861–4871. https://doi.org/10.1002/jgrb.50358

Mankhemthong N, Doser DI, Pavlis TL (2013) Interpretation of gravity and magnetic data and development of two-dimensional cross-sectional models for the Border Ranges fault system, south-central Alaska. Geosphere 9:242–259. https://doi.org/10.1130/GES00833.1

Marc O, Hovius N, Meunier P et al (2015) Transient changes of landslide rates after earthquakes. Geology 43:883–886. https://doi.org/10.1130/G36961.1

Markland JT (1972) A useful technique for estimating the stability of rock slopes when the rigid wedge slide type type of failure is expected. Imper Coll Sci Technol

McColl ST (2012) Paraglacial rock-slope stability. Geomorphology 153–154:1–16. https://doi.org/10.1016/j.geomorph.2012.02.015

McColl ST, Draebing D (2019) Rock slope instability in the proglacial zone: state of the art. In: Heckmann T, Morche D (eds) Geomorphology of proglacial systems. Springer International Publishing, Cham, pp 119–141

McDougall S, Hungr O (2004) A model for the analysis of rapid landslide motion across three-dimensional terrain. Can Geotech J 41:1084–1097. https://doi.org/10.1139/t04-052

Miller DJ (1960) Giant waves in Lituya Bay Alaska. Geol Surv Prof Paper 354-C

Moore J, Gischig V, Amann F et al (2012) Earthquake-triggered rock slope failures: damage and site effects. In: Landslides and Engineered Slopes: Protecting Society Through Improved Understanding

Moser M, Amann F, Meier J, Weidner S (2017) Tiefgreifende Hangdeformationen der Alpen. Springer Fachmedien Wiesbaden, Wiesbaden

Nichols TC (1980) Rebound, its nature and effect on engineering works. Q J Eng GeolHydrogeol 13:133–152. https://doi.org/10.1144/GSL.QJEG.1980.013.03.01

Nokleberg WJ, Plafker G, Lull JS et al (1989) Structural analysis of the Southern Peninsular, Southern Wrangellia, and Northern Chugach Terranes Along the Trans-Alaska Crustal Transect, Northern Chugach Mountains, Alaska. J Geophys Res 94:4297–4320. https://doi.org/10.1029/JB094iB04p04297

Oppikofer T, Jaboyedoff M, Keusen H-R (2008) Collapse at the eastern Eiger flank in the Swiss Alps. Nature Geosci 1:531–535. https://doi.org/10.1038/ngeo258

Pastick NJ, Jorgenson MT, Wylie BK et al (2015) Distribution of near-surface permafrost in Alaska: estimates of present and future conditions. Remote Sens Environ 168:301–315. https://doi.org/10.1016/j.rse.2015.07.019

Penna I, Böhme M, Hermanns R (2017) Dynamic modelling with DAN3D of Stampa scenario 3A. NGU

Petley D (2022) The 17 September 2022 rock avalanche at Lamplugh Glacier in Alaska. In: The Landslide Blog. https://blogs.agu.org/landslideblog/2022/09/23/lamplugh-glacier-1/. Accessed 19 Oct 2023

Plafker G, Nokleberg WJ, Lull JS (1989) Bedrock geology and tectonic evolution of the Wrangellia, Peninsular, and Chugach Terranes along the Trans-Alaska Crustal Transect in the Chugach Mountains and Southern Copper River Basin, Alaska. J Geophys Res 94:4255–4295. https://doi.org/10.1029/JB094iB04p04255

Post A (1967) The Alaska earthquake, March 27, 1964: Effects on the hydrologic regimen. Geological Survey Publication, U.S. https://doi.org/10.3133/pp544

Rantanen M, Karpechko AYu, Lipponen A et al (2022) The Arctic has warmed nearly four times faster than the globe since 1979. Commun Earth Environ 3:168. https://doi.org/10.1038/s43247-022-00498-3

Rechberger C, Fey C, Zangerl C (2021) Structural characterisation, internal deformation, and kinematics of an active deep-seated rock slide in a valley glacier retreat area. Eng Geol 286:106048. https://doi.org/10.1016/j.enggeo.2021.106048

Rodríguez CE, Bommer JJ, Chandler RJ, (1999) Earthquake-induced landslides: 1980–1997. Soil Dyn Earthq Eng 18:325–346. https://doi.org/10.1016/S0267-7261(99)00012-3

Si P, Aaron J, McDougall S et al (2017) A non-hydrostatic model for the numerical study of landslide-generated waves. Landslides 15:711–726. https://doi.org/10.1007/s10346-017-0891-y

Slaymaker O (2009) The future of geomorphology: the future of geomorphology. Geogr Compass 3:329–349. https://doi.org/10.1111/j.1749-8198.2008.00178.x

Sosio R, Crosta GB, Hungr O (2008) Complete dynamic modeling calibration for the Thurwieser rock avalanche (Italian Central Alps). Eng Geol 100:11–26. https://doi.org/10.1016/j.enggeo.2008.02.012

Sosio R, Crosta GB, Chen JH, Hungr O (2012) Modelling rock avalanche propagation onto glaciers. Quatern Sci Rev 47:23–40. https://doi.org/10.1016/j.quascirev.2012.05.010

Spreafico MC, Sternai P, Agliardi F (2021) Paraglacial rock-slope deformations: sudden or delayed response? Insights from an integrated numerical modelling approach. Landslides 18:1311–1326. https://doi.org/10.1007/s10346-020-01560-x

Stead D, Wolter A (2015) A critical review of rock slope failure mechanisms: the importance of structural geology. J Struct Geol 74:1–23. https://doi.org/10.1016/j.jsg.2015.02.002

Stock GM, Martel SJ, Collins BD, Harp EL (2012) Progressive failure of sheeted rock slopes: the 2009–2010 Rhombus Wall rock falls in Yosemite Valley, California, USA: progressive failure of sheeted rock slopes. Earth Surf Process Landforms 37:546–561. https://doi.org/10.1002/esp.3192

Storni E, Hugentobler M, Manconi A, Loew S (2020) Monitoring and analysis of active rockslide-glacier interactions (Moosfluh, Switzerland). Geomorphology 371:107414. https://doi.org/10.1016/j.geomorph.2020.107414

Stover CW, Coffman JL (1993) Seismicity of the United States 1568–1989 (revised)

Terzaghi K (1950) Mechanism of landslides. In: Paige S (ed) Application of geology to engineering practice. Geological Society of America, New York, N. Y., pp 83–123
The Homer News (1967) Water for east element
Tsutaki S, Fujita K, Nuimura T et al (2019) Contrasting thinning patterns between lake- and land-terminating glaciers in the Bhutanese Himalaya. Cryosphere 13:2733–2750. https://doi.org/10.5194/tc-13-2733-2019
U.S. Geological Survey (2020) M 9.2 - 1964 Prince William Sound Earthquake, Alaska. https://earthquake.usgs.gov/earthquakes/eventpage/iscgem869809/shakemap/intensity. Accessed 31 Jul 2023
U.S. Geological Survey (2022) Earthquake Hazards Program: search earthquake catalog. https://earthquake.usgs.gov/earthquakes/search/. Accessed 22 Apr 2022
VanLooy J, Forster R, Ford A (2006) Accelerating thinning of Kenai Peninsula glaciers. Alaska Geophys Res Lett 33:L21307. https://doi.org/10.1029/2006GL028060
Wiles GC, Calkin PE (1992) Reconstruction of a debris-slide-initiated flood in the southern Kenai Mountains, Alaska. Geomorphology 5:535–546. https://doi.org/10.1016/0169-555X(92)90024-I
Wilson FH, Hults CP, Mull CG, Karl SM (2015) Geologic map of Alaska. U.S. Geological Survey Scientific Investigations, Map 3340, scale: 1:1,584,000
Wyllie DC, Norrish NI (1996) Landslides: investigation and mitigation. Chapter 14 - Rock strength properties and their measurement. Transportation Research Board Special Report. Issue Number: 247, ISSN: 0360-859X
Wyllie DC, Mah CW (2004) Rock slope engineering: civil and mining, 4th edn. Spon Press, London, New York
Yang W, Qi W, Wang M et al (2017) Spatial and temporal analyses of post-seismic landslide changes near the epicentre of the Wenchuan earthquake. Geomorphology 276:8–15. https://doi.org/10.1016/j.geomorph.2016.10.010
Yang R, Hock R, Kang S et al (2020) Glacier mass and area changes on the Kenai Peninsula, Alaska, 1986–2016. J Glaciol 66:603–617. https://doi.org/10.1017/jog.2020.32
Yang R, Hock R, Kang S et al (2022) Glacier surface speed variations on the Kenai Peninsula, Alaska, 2014–2019. JGR Earth Surf 127:e2022JF006599. https://doi.org/10.1029/2022JF006599
Zhang G, Bolch T, Yao T et al (2023) Underestimated mass loss from lake-terminating glaciers in the greater Himalaya. Nat Geosci 16:333–338. https://doi.org/10.1038/s41561-023-01150-1

**Emilie Lemaire** (✉) · **Anja Dufresne** · **Pooya Hamdi** · **Florian Amann**
Institute of Engineering Geology and Hydrogeology, RWTH-Aachen University, Aachen, Germany

**Emilie Lemaire**
Email: lemaire@lih.rwth-aachen.de

**Bretwood Higman**
Ground Truth Trekking, Seldovia, AK, USA

**Gabriel J. Wolken**
Division of Geological & Geophysical Surveys, Fairbanks, AK, USA

**Gabriel J. Wolken**
International Arctic Research Center, University of Alaska Fairbanks, Fairbanks, AK, USA